Special Issue Multiscale Simulations for Materials

特集

Research Report

Lattice Boltzmann Method and its Application to Flow Analysis in Porous Media

Hidemitsu Hayashi

格子ボルツマン法とその多孔体中の流れ解析への応用

林秀光

Abstract

Under the existence of an external force, a lattice Boltzmann method (LBM) is derived by discretizing the Boltzmann equation with respect to velocity, space and time. The LBM is applied to simulations of flow through three-dimensional porous structures of Nafion polymer membranes. Geometry data of Nafion are constructed based on the result of a dissipative particle dynamics simulation for three values of water content, 10%, 20%, and 30%, and are used as the geometry input for the LBM. Using Darcy's law, the permeability of the porous structure is extracted from the results obtained by two kinds of LBM, the LBM under an external force and the LBM under a pressure gradient. The two types of LBM are found to produce permeabilities that are in good agreement with each other.

Keywords Computer simulation, Fluid dynamics, Porous media, Lattice Boltzmann method

要　旨

連続のボルツマン方程式を，速度・空間・時間の各座標に関して離散化する事により，外力が存在する場合の格子ボルツマン法を導出した。この格子ボルツマン法を，3次元的な多孔質構造を有する高分子電解質膜Nafionに適用した。格子ボルツマン法の入力データとして必要なNafionの構造は，散逸粒子動力学法により3つの含水率(10%, 20%, 30%)に対して決定されたものを用いた。流れの駆動力として圧力勾配を用いた場合と外力を用いた場合の2種類の格子ボルツマン法による計算を実施し，Darcy則を用いてNafionの透過係数を算出した。これら2種類の計算結果から得られた透過係数は，たがいに良く一致した。

キーワード　コンピュータシミュレーション，流体力学，多孔体，格子ボルツマン法

特集

1. Introduction

The Lattice Boltzmann method (LBM) [1, 2] has recently attracted considerable attention in the anticipation of simulating fluid flows in porous media and in multiphase states, which are difficult problems to solve by conventional computational fluid dynamics techniques.

This method and its predecessor, the Lattice-Gas method (LGM), were found to be easily applied to fluid flows in porous media immediately after their discovery. [3] Buckles et al. [4] and Auzerais et al. [5] investigated flow through porous rocks using the LBM and calculated the permeability of these rocks [6] , i.e. the fundamental physical quantity of porous media. They found the calculated value of permeability to be in good agreement with that obtained experimentally.

In the present study, we apply the LBM to flow analysis of Nafion polymer membranes, the best-known proton conducting electrolyte of fuel cells. The greatest problem in applying the LBM is determination of the structure of the porous media. Two possible approaches to this problem are: (i) constructing a three-dimensional digital image of the pore space using X-ray computer tomography (CT); (ii) mimicking by simulation the manufacturing process used to create the actual porous material. We cannot apply the first approach to Nafion polymer membranes, because the resolution of X-ray CT, a few μm at best, is insufficient to resolve the nanoscale pore structure of Nafion. Hence, we adopt the second approach, and fabricate the morphology of Nafion polymer membranes using a dissipative particle dynamics (DPD) technique. [7, 8]

2. Lattice Boltzmann method

Historically, the Lattice Boltzmann method developed from the Lattice-Gas method. [9] Recently, the LBM is proved to be a special discretized form of the continuous Boltzmann equation (CBE). [10, 11] We derive an LBM with an external force from the CBE in **Sec. 2.1**. We formulate the method of applying the LBM to porous media in **Sec. 2.2**.

2.1 From Boltzmann equation to LBM

For the case in which an external force $\mathbf{f}$ exists, the continuous Boltzmann equation with the BGK approximation [12] for the collision term is written as

$$\frac{\partial f}{\partial t} + \mathbf{e} \bullet \frac{\partial}{\partial \mathbf{r}} f + \mathbf{f} \bullet \frac{\partial}{\partial \mathbf{e}} f = -\frac{1}{\tau} \left(f - f^{eq} \right), \quad (1)$$

where f is the distribution function of a spatial coordinate $\mathbf{r}$ and a velocity $\mathbf{e}$, and τ is the relaxation time. The local equilibrium distribution function f^{eq} is described by the Maxwell distribution:

$$f^{eq} = \frac{\rho}{(2\pi RT)^{\frac{D}{2}}} \exp\left[-\frac{(\mathbf{e}-\mathbf{u})^2}{2RT} \right]. \quad (2)$$

Here, R is the gas constant; T is the temperature; D is the spatial dimension. The local density ρ and the local velocity $\mathbf{u}$ are calculated as the moments of the distribution function:

$$\rho = \int f \, d\mathbf{e}, \quad (3)$$

$$\rho \mathbf{u} = \int \mathbf{e} f \, d\mathbf{e}. \quad (4)$$

Since in this study we are considering the case in which deviation from the local equilibrium is small, the derivative of the distribution function with respect to the velocity in Eq.(1) can be approximated as [13, 14]

$$\frac{\partial}{\partial \mathbf{e}} f \approx \frac{\partial}{\partial \mathbf{e}} f^{eq} = -\frac{(\mathbf{e}-\mathbf{u})}{RT} f^{eq}. \quad (5)$$

Consequently, we obtain the following equation as the starting point for deriving the LBM:

$$\frac{\partial f}{\partial t} + \mathbf{e} \bullet \frac{\partial}{\partial \mathbf{r}} f - \frac{\mathbf{f} \bullet (\mathbf{e}-\mathbf{u})}{RT} f^{eq} = -\frac{1}{\tau} \left(f - f^{eq} \right). \quad (6)$$

The LBM with an external force is derived through the discretization of Eq.(6) with respect to the velocity, spatial and time coordinates. [10, 11, 15–17] We first execute the discretization in the velocity space:

$$\frac{\partial f_i}{\partial t} + \mathbf{e}_i \bullet \frac{\partial}{\partial \mathbf{r}} f_i - \frac{\mathbf{f} \bullet (\mathbf{e}_i - \mathbf{u})}{RT} f_i^{eq} = -\frac{1}{\tau} \left(f_i - f_i^{eq} \right), \quad (7)$$

where $\mathbf{e}_i$ is the discrete velocities, the distribution function f_i and the local equilibrium distribution function f_i^{eq} are defined as

$$f_i \equiv w_i \left(2\pi RT\right)^{\frac{D}{2}} \exp\left[\frac{\mathbf{e}_i^2}{2RT}\right] f\left(\mathbf{r}, \mathbf{e}_i\right), \tag{8}$$

$$f_i^{eq} \equiv w_i \left(2\pi RT\right)^{\frac{D}{2}} \exp\left[\frac{\mathbf{e}_i^2}{2RT}\right] f^{eq}\left(\mathbf{u}, \mathbf{e}_i\right), \tag{9}$$

$$= \rho w_i \exp\left[-\frac{\left(u^2 - 2\mathbf{e}_i \bullet \mathbf{u}\right)}{2RT}\right], \tag{10}$$

$$\approx \rho w_i \left[1 + \frac{\mathbf{e}_i \bullet \mathbf{u}}{RT} + \frac{\left(\mathbf{e}_i \bullet \mathbf{u}\right)^2}{2\left(RT\right)^2} - \frac{u^2}{2RT}\right]; \tag{11}$$

and w_i are the weight coefficients.

The discrete velocities $\mathbf{e}_i$ and the weight coefficients w_i are determined so as to recover the Navier-Stokes equation from the LBM in the long-wage-length and low-frequency limit. Therefore, the necessary conditions imposed on $\mathbf{e}_i$ and w_i are as follows: [18]

$$\sum_i w_i = 1, \tag{12}$$

$$\sum_i w_i e_{i\alpha} e_{i\beta} \propto \delta_{\alpha,\beta}, \tag{13}$$

$$\sum_i w_i e_{i\alpha} e_{i\beta} e_{i\gamma} e_{i\delta} \tag{14}$$

$$\propto \left(\delta_{\alpha,\beta}\delta_{\gamma,\delta} + \delta_{\alpha,\gamma}\delta_{\beta,\delta} + \delta_{\alpha,\delta}\delta_{\beta,\gamma}\right).$$

For the two-dimensional problem, the nine-velocity model (D2Q9):

$$\mathbf{e}_i = \begin{cases} (0,0), & (i=0) \\ (\pm 1, 0)c, (0, \pm 1)c, & (i = 1, ..., 4) \\ (\pm 1, \pm 1)c, & (i = 5, ..., 8) \end{cases} \tag{15}$$

$$w_i = \begin{cases} 4/9, & (i=0) \\ 1/9, & (i = 1, ..., 4) \\ 1/36, & (i = 5, ..., 8) \end{cases} \tag{16}$$

is frequently used.

For the three-dimensional problem, several velocity models have been proposed, including the fifteen-velocity model (D3Q15), the nineteen-velocity model (D3Q19), and the twenty-seven-velocity model (D3Q27). [19] We will use the D3Q15 model in a latter section, where $\mathbf{e}_i$ and w_i are given by

$$\mathbf{e}_i = \begin{cases} (0,0,0), & (i=0) \\ (\pm 1, 0, 0)c, (0, \pm 1, 0)c, & \\ \quad (0, 0, \pm 1)c, & (i = 1, .., 6) \\ (\pm 1, \pm 1, \pm 1)c, & (i = 7, ..., 14) \end{cases} \tag{17}$$

$$w_i = \begin{cases} 2/9, & (i=0) \\ 1/9, & (i = 1, .., 6) \\ 1/72, & (i = 7, ..., 14). \end{cases} \tag{18}$$

In Eqs. (15,17), c is defined by

$$c \equiv \sqrt{3RT}. \tag{19}$$

We can easily prove that the following relations are satisfied for every pair of $\mathbf{e}_i$ and w_i in Eqs.(15,16) and Eqs.(17,18):

$$\sum_i w_i = 1, \tag{20}$$

$$\sum_i w_i e_{i\alpha} e_{i\beta} = \frac{1}{3} c^2 \delta_{\alpha,\beta}, \tag{21}$$

$$\sum_i w_i e_{i\alpha} e_{i\beta} e_{i\gamma} e_{i\delta} \tag{22}$$

$$= \frac{1}{9} c^4 \left(\delta_{\alpha,\beta}\delta_{\gamma,\delta} + \delta_{\alpha,\gamma}\delta_{\beta,\delta} + \delta_{\alpha,\delta}\delta_{\beta,\gamma}\right).$$

Thus, we have confirmed that these pairs of $\mathbf{e}_i$ and w_i obey the condition of Eqs.(12,13,14).

We require that the Boltzmann equation discretized with respect to the velocity coordinate, Eq.(7), satisfies conservation of mass and momentum at each spatial point:

$$\sum_i f_i = \sum_i f_i^{eq} = \rho, \tag{23}$$

$$\sum_i \mathbf{e}_i f_i = \sum_i \mathbf{e}_i f_i^{eq} = \rho \mathbf{u}. \tag{24}$$

We have used Eqs.(11,20,21) to derive the sum rules for f_i^{eq} in Eqs.(23,24). Recently, the Boltzmann equation discretized with respect to the velocity coordinate has been solved directly by a finite difference method. [20]

In the next step, we perform the discretization of Eq.(7) with respect to the spatial and time coordinates. Let us rewrite Eq.(7) as follows:

$$\frac{\partial f_i}{\partial t} + \mathbf{e}_i \bullet \frac{\partial}{\partial \mathbf{r}} f_i = -\frac{1}{\tau}\left(f_i - f_i^{eq}\right) - F_i, \tag{25}$$

$$F_i \equiv -\frac{\mathbf{f} \bullet \left(\mathbf{e}_i - \mathbf{u}\right)}{RT} f_i^{eq}. \tag{26}$$

Integrating both side of Eq.(25) from t to $t+\delta_t$, the left-hand side is reduced to

$$\int_t^{t+\delta_t}\left(\frac{\partial f_i}{\partial t}+\mathbf{e}\bullet\frac{\partial}{\partial \mathbf{r}}f_i\right)dt = f_i\left(\mathbf{x}+\mathbf{e}_i\delta_t, t+\delta_t\right)-f_i\left(\mathbf{x},t\right), \tag{27}$$

and the right-hand side becomes

$$\begin{aligned}\int_t^{t+\delta_t}&\left(-\frac{1}{\tau}\left(f_i-f_i^{eq}\right)-F_i\right)dt \\ &= \frac{\delta_t}{2}\left[-\frac{1}{\tau}\left(f_i-f_i^{eq}\right)-F_i\right]\Big|_{t+\delta_t} \\ &+ \frac{\delta_t}{2}\left[-\frac{1}{\tau}\left(f_i-f_i^{eq}\right)-F_i\right]\Big|_{t}+O(\delta_t^3)\end{aligned} \tag{28}$$

in the second order approximation with respect to δ_t. We have used the trapezoidal rule to derive Eq.(28) and then obtain

$$\begin{aligned}&f_i\left(\mathbf{x}+\mathbf{e}_i\delta_t, t+\delta_t\right)-f_i\left(\mathbf{x},t\right) \\ &= \frac{\delta_t}{2}\left[-\frac{1}{\tau}\left(f_i-f_i^{eq}\right)-F_i\right]\Big|_{t+\delta_t} \\ &+ \frac{\delta_t}{2}\left[-\frac{1}{\tau}\left(f_i-f_i^{eq}\right)-F_i\right]\Big|_{t}+O(\delta_t^3).\end{aligned} \tag{29}$$

To translate Eq.(29) into the explicit form, we introduce $\widetilde{f}_i$ defined by

$$\tilde{f}_i \equiv f_i+\frac{\delta_t}{2\tau}\left(f_i-f_i^{eq}\right)+\frac{\delta_t}{2}F_i. \tag{30}$$

Using $\widetilde{f}_i$, Eq.(29) is expressed as

$$\begin{aligned}&\tilde{f}_i\left(\mathbf{x}+\mathbf{e}_i\delta_t, t+\delta_t\right)-\tilde{f}_i\left(\mathbf{x},t\right) \\ &= \delta_t\left[-\frac{1}{\tau}\left(f_i-f_i^{eq}\right)-F_i\right]\Big|_{t} \\ &= -\frac{\delta_t}{\tau+0.5\delta_t}\left(\tilde{f}_i-f_i^{eq}\right)-\frac{\tau\delta_t}{\tau+0.5\delta_t}F_i.\end{aligned} \tag{31, 32}$$

Introducing the dimensionless relaxation time $\widetilde{\tau}$ through

$$\widetilde{\tau}=\frac{\tau}{\delta_t}+0.5, \tag{33}$$

Eq.(32) becomes

$$\begin{aligned}&\tilde{f}_i\left(\mathbf{x}+\mathbf{e}_i\delta_t, t+\delta_t\right)-\tilde{f}_i\left(\mathbf{x},t\right) \\ &= -\frac{1}{\widetilde{\tau}}\left(\tilde{f}_i-f_i^{eq}\right) \\ &+ \frac{(\widetilde{\tau}-0.5)}{\widetilde{\tau}}\delta_t\frac{\mathbf{f}\bullet(\mathbf{e}_i-\mathbf{u})}{RT}f_i^{eq}.\end{aligned} \tag{34}$$

Through the use of Eqs.(20,21,23,24,26,34), we confirm that $\widetilde{f}_i$ satisfies the following relations:

$$\sum_i \tilde{f}_i=\sum_i f_i=\sum_i f_i^{eq}=\rho, \tag{35}$$

$$\begin{aligned}\sum_i \mathbf{e}_i\tilde{f}_i &= \sum \mathbf{e}_i f+\frac{\delta_t}{2}\sum_i \mathbf{e}_i F_i \\ &= \sum \mathbf{e}_i f_i^{eq}+\frac{\delta_t}{2}\sum_i \mathbf{e}_i F_i=\rho\mathbf{u}-\frac{\delta_t}{2}\rho\mathbf{f}.\end{aligned} \tag{36}$$

The lattice Boltzmann method with an external force $\mathbf{f}$ is composed of Eqs.(34,35,36) and Eq.(11). From the definition of $\widetilde{\tau}$, Eq.(33), we find that $\widetilde{\tau}$ must satisfy the constraint $\widetilde{\tau}>0.5$.

Prior to the works of He et al.[10, 11, 13] , the LBM with an external force had been proposed based on empirical studies, and recently a few papers on this subject have been published. [21, 22] However, as we have examined in this section, the LBM with an external force can be derived consistently from the continuous Boltzmann equation in the deductive method.

2.2 Application of LBM to porous media

The LBM derived in **Sec.2.1** takes the density and the velocity as independent variables. To simulate fluid flow in porous media, we utilize an LBM for incompressible fluid,[23] in which pressure and velocity are independent variables. This LBM is convenient for confirming the conservation of flow late, which, for an incompressible fluid, must be constant over a porous media. The LBM taking the velocity $\mathbf{u}$ and the pressure p as independent variables is:

$$\begin{aligned}&f_i\left(\mathbf{x}+\mathbf{e}_i\delta_t, t+\delta_t\right)-f_i\left(\mathbf{x},t\right) \\ &= -\frac{1}{\tau}\left(f_i-f_i^{eq}\right)-\frac{\tau-0.5}{\tau}\delta_t F_i,\end{aligned} \tag{37}$$

where we have expressed the dimensionless relaxation time introduced in Eq.(33) by τ. The local equilibrium distribution function f_i^{eq} and the ex-

ternal force term F_i are:

$$f_i^{eq} = w_i \left[\tilde{p} + \frac{\mathbf{e}_i \bullet \mathbf{u}}{RT} + \frac{(\mathbf{e}_i \bullet \mathbf{u})^2}{2(RT)^2} - \frac{u^2}{2RT} \right], \tag{38}$$

$$F_i = -\frac{\mathbf{f} \bullet (\mathbf{e}_i - \mathbf{u})}{RT} f_i^{eq}, \tag{39}$$

$$\tilde{p} = \frac{1}{c_s^2 \rho_0} p = \sum_i f_i, \tag{40}$$

$$\mathbf{u} = \sum_i \mathbf{e}_i f_i + 0.5 \mathbf{f} \delta_t, \tag{41}$$

where p is the pressure, $\tilde{p}$ is the dimensionless pressure, c_s is the sound velocity, and ρ_0 is the density of the incompressible fluid.

Using the Chapman-Enskog expansion, [24] we can derive the macroscopic hydrodynamic equations from the LBM for an incompressible fluid in the region of low Knudsen number and low Mach number:[23]

$$\frac{1}{c_s^2 \rho_0} \frac{\partial p}{\partial t} + \nabla \bullet \mathbf{u} = 0, \tag{42}$$

$$\frac{\partial \mathbf{u}}{\partial t} + \mathbf{u} \bullet \nabla \mathbf{u} = -\frac{1}{\rho_0} \nabla p + \nu \nabla^2 \mathbf{u} + \mathbf{f}. \tag{43}$$

In all of the velocity models (D2Q9, D3Q15, D3Q19, D3Q27) mentioned in **Sec.2.1**, the kinematic viscosity ν and the sound velocity c_s are given by

$$\nu = \frac{2\tau - 1}{6} c^2 \delta_t \ ; \quad c_s = \frac{c}{\sqrt{3}}. \tag{44}$$

For the case in which the external force $\mathbf{f}$ is conservative, the external force is given using the potential Ω:

$$\mathbf{f} = -\nabla \Omega. \tag{45}$$

Then, Eq.(43) becomes

$$\frac{\partial \mathbf{u}}{\partial t} + \mathbf{u} \bullet \nabla \mathbf{u} = -\frac{1}{\rho_0} \nabla (p + \rho_0 \Omega) + \nu \nabla^2 \mathbf{u}. \tag{46}$$

Equations (43,46) indicate that for the fluid flow generated by a constant pressure gradient ∇p, such as the Poiseuille flow, the fluid velocity $\mathbf{u}$ is the same as that driven by the following constant external force $\mathbf{f}$:

$$\mathbf{f} = -\frac{1}{\rho_0} \nabla p = -c_s^2 \nabla \tilde{p} = -\frac{c^2}{3} \nabla \tilde{p}. \tag{47}$$

Permeability, the fundamental physical quantity of porous media, is defined using Darcy's law:[6]

$$\langle \mathbf{u} \rangle = -\frac{K}{\mu} (\nabla p - \rho_0 \mathbf{f}), \tag{48}$$

where $\mathbf{u}$ is the fluid velocity, $\langle \cdots \rangle$ is the average over the porous media, ∇p is the pressure gradient, $\rho_0 \mathbf{f}$ is the external force operating on the unit volume of the fluid, and μ is the viscosity related to the kinematic viscosity ν through $\nu = \mu / \rho_0$.

As we will see in the next section, the pressure in porous media shows a complex position dependence and its gradient is not constant. Nevertheless, Darcy's law as given in Eq.(48) indicates that the averaged fluid velocity generated by the averaged pressure gradient ∇p is the same as that derived using the constant external force $\mathbf{f}$ defined in Eq.(47). We will verify the identity between the effect of the pressure gradient and that of the external force stated in the Darcy's law through calculations of permeability in **Sec.3**.

For the purpose of numerical calculations in the next section, it is convenient to introduce the dimensionless permeability K_{tpl}, which is related to the permeability K for porous media having the shape of a cube with side length L_c:

$$K_{tpl} = \frac{1}{L_c^2} K = \frac{3\tilde{u}^2}{Re \Delta \tilde{p}}, \tag{49}$$

where the dimensionless velocity $\tilde{u}$, the Reynolds number Re, and the dimensionless pressure difference $\Delta \tilde{p}$ are defined by

$$\tilde{u} = \frac{u}{c} \ , \quad Re = \frac{u L_c}{\nu} \ , \quad \Delta \tilde{p} = L_c \times |\nabla \tilde{p}| \ . \tag{50}$$

Hereafter, we use the lattice unit defined through $c = \delta_t = 1$.

3. Flow analysis in porous media

In this section, we apply the LBM developed in **Sec. 2** to three-dimensional porous structures of Nafion polymer membranes. The structures of Nafion constructed as a result of a dissipative particle dynamics simulation [8] are shown in **Fig. 1** for three values of water content, 10%, 20%, and 30%. Polymer molecules of Nafion 117 occupy gray

regions in Fig. 1. A cube surrounding the gray region, whose edge length is 15nm, is divided into a $40 \times 40 \times 40$ voxel lattice, and the vertices of the voxels are used as the lattice points of the LBM.

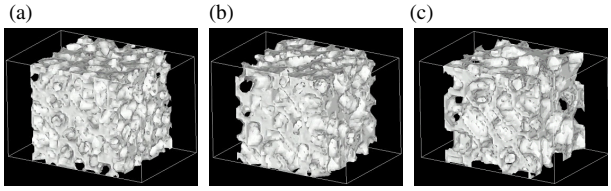

Fig. 1 Structure of Nafion obtained by the DPD simulation for three values of water content, 10 vol % (a), 20 vol % (b), and 30 vol % (c).

We impose the bounce back boundary condition (BBBC) [25] at the lattice points occupied by the polymer molecules. At the inlet and outlet, we prepare a runway having a width of 11 lattice points along the pressure gradient or the external force. The inflow and outflow boundary conditions are constant pressure on the inlet and outlet plane [25] for the flow generated by the pressure gradient, and the inlet and the outlet are connected by the periodic boundary condition for the flow driven by the external force. In this study, we adopted the fifteen-velocity model (D3Q15) defined in **Sec.2.1**. Hereafter, the flow generated by the pressure gradient and the flow driven by the external force are designated as FGPG and FDEF, respectively.

The calculated fluid velocity vectors are shown in **Fig. 2**. The magnitude of the velocity vector is represented by color, where the highest velocity is red and the lowest velocity is blue. Figures 2(a,b,c) are the results for FGPG, and Figs. 2(a',b',c') are those for FDEF. In these figures, a quarter of the region occupied by polymer molecules is removed to display the fluid velocity. In this calculation, the kinematic viscosity ν is 0.05; the pressure difference between the inlet and outlet, $\Delta\tilde{p}$, is 0.5 for FGPG; the magnitude of the external force for FDEF is estimated from the relation: $\tilde{f} = 3Lf = \Delta\tilde{p}$, where $L(= 62)$ is the number of lattice points along the flow direction. From these figures, we can see that the result for FGPG and that for FDEF are in good agreement.

Figure 3 shows the calculated pressure distribution in the porous media for FGPG, which is averaged on the plane perpendicular to the flow direction. The kinematic viscosity ν is 0.05 and the pressure difference between the inlet and outlet, $\Delta\tilde{p}$, is 0.5. From this figure, we find that: (1) almost all of the pressure change (the pressure-loss) occurs inside the porous media; (2) the pressure can be considered as constant at the runway; (3) the pressure distribution shows a complex change along the flow direction inside the porous media.

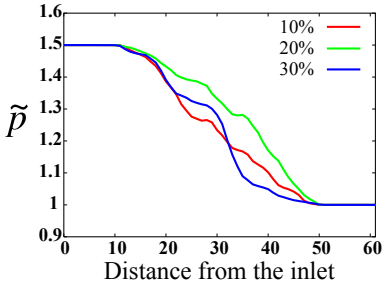

Fig. 2 Calculated velocity vectors in Nafion. The magnitude of the velocity vector is represented by color, where the largest velocity is red and the lowest velocity is blue. Results are compared for the flow generated by the pressure gradient (a,b,c) and the flow driven by the external force (a',b',c'). $\nu = 0.05, \Delta\tilde{p} = \tilde{f} = 0.05$.

Fig. 3 Calculated pressure distribution averaged on the plane perpendicular to the flow direction in Nafion for three values of water content. $\nu = 0.05$, $\Delta\tilde{p} = 0.05$.

Figure 4 shows the velocity distribution averaged on the plane perpendicular to the flow direction. In this figure, results are compared for FGPG (a) and FDEF (b). Parameters of the flow

are as follows: $\nu = 0.05$ in both Fig. 4(a) and Fig. 4(b); $\Delta\tilde{p} = 0.5$ in Fig. 4(a) where $\Delta\tilde{p}$ is the difference in pressure between the inlet and the outlet; $\tilde{f} = 3Lf = \Delta\tilde{p}$ in Fig. 4(b). Figure 4 shows that the result for FGPG is in good agreement with that for FDEF and the average flow velocity is constant in the region between the inlet and the outlet. The constant velocity indicates conservation of flow rate, and the LBM satisfies one of the necessary constraints on the incompressible flow.

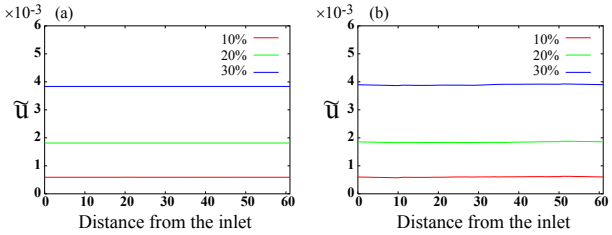

Fig. 4 Calculated velocity distribution averaged on the plane perpendicular to the flow direction. Results are compared for the flow generated by the pressure gradient (a) and the flow driven by the external force (b). $\nu = 0.05, \Delta\tilde{p} = \tilde{f} = 0.5$.

Using the calculated velocity $\tilde{u}$, we can estimate the permeability from Eq.(49). **Figures 5(a)** and **5(b)** show the calculation results for the dimensionless permeability K_{tpl}. Figure 5(a) shows the dependence of K_{tpl} on the pressure difference between the inlet and the outlet. Figure 5(b) shows the dependence of K_{tpl} on the magnitude of the external force. In this figure, the abscissa $\tilde{f}$ is defined through the relation: $\tilde{f} = 3Lf(= \Delta\tilde{p})$. In these figures, the kinematic viscosity is fixed at $\nu = 0.1$. Two results for FGPG and FDEF are in good agreement. The permeability must be independent of the pressure gradient or the external force used in the calculation thereof, because, according to Darcy's law, the permeability is an intrinsic quantity of each porous media . As shown in Fig. 5(a) and Fig. 5(b), the LBM produces the correct result for this requirement for the calculated permeability.

Changing the magnitude of the kinematic viscosity, we have calculated the dimensionless permeability K_{tpl}, and the result is given in **Fig. 6**. The

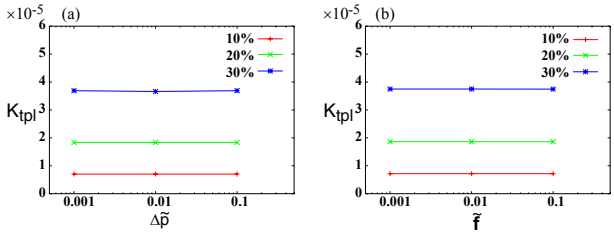

Fig. 5 Dependence of dimensionless permeability on the pressure gradient and the external force. Results are compared for the flow generated by the pressure gradient (a) and the flow driven by the external force (b). $\nu = 0.1$.

dimensionless pressure difference $\Delta\tilde{p}$ in Fig. 6(a) and the magnitude of the external force in Fig. 6(b) are fixed under the relationship: $\Delta\tilde{p} = \tilde{f} = 0.01$. Here, the results for FGPG in Fig. 6(a) and for FDEF in Fig. 6(b) are in good agreement, and the calculated permeability depends strongly on the kinematic viscosity of the fluid. According to Darcy's law, the second item is unphysical, because the permeability is an intrinsic quality of the porous media and must be independent of the kinematic viscosity of the fluid used in the calculation.

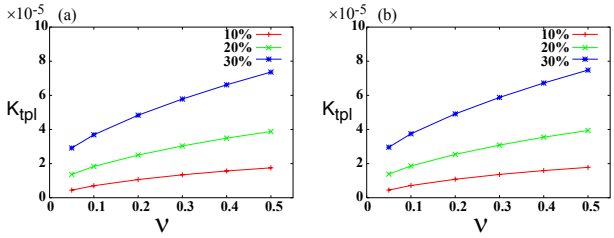

Fig. 6 Dependence of dimensionless permeability on the fluid viscosity. Results are compared for the flow generated by the pressure gradient (a) and the flow driven by the external force (b). $\Delta\tilde{p} = \tilde{f} = 0.01$.

The problem wherein the permeability varies with the fluid viscosity has been investigated by Ferréol et al. [26] , and has been interpreted to originate from insufficient resolution of the underling lattice of the LBM. In order to confirm this interpretation, we increased the resolution by preparing a fine grid, in which each gray region in Fig. 1 is divided into an $80 \times 80 \times 80$ voxel lattice, and cal-

culated the permeability using the fine grid. The result is shown in **Fig. 7**. We understand from this figure that the viscosity dependence decreases with the increase in the grid resolution, and the interpretation mentioned above is confirmed. In addition, Fig. 7 indicates that the dependence of the permeability on the grid resolution decreases as the viscosity decreases.

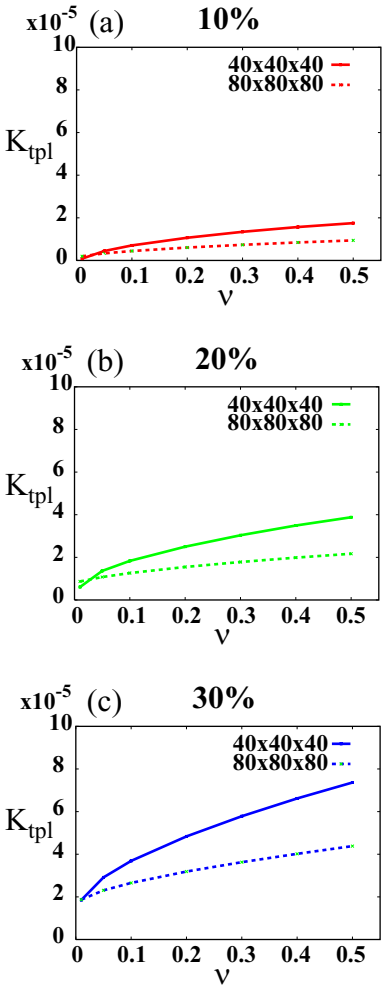

Fig. 7 Dependence of dimensionless permeability on the fluid viscosity and the grid resolution. The water content of Nafion is 10% for (a), 20% for (b), 30% for (c). $\Delta\tilde{p} = 0.01$.

4. Conclusions

We have developed the LBM with an external force for incompressible fluid, in which the independent variables are pressure and velocity. Using this LBM, we can impose the periodic boundary condition on the inlet and outlet of the flow driven by the external force. This is an advantage of the LBM with an external force, because we can easily code the periodic boundary condition to be applicable to any velocity model, while the fluid mechanical boundary condition must be prepared for each velocity model. In addition, we have performed simulations of flow through three-dimensional porous structures of Nafion polymer membranes using two kinds of LBM, i.e. LBM with and without an external force. The two LBMs produce permeabilities that are in good agreement with each other, and the LBM is confirmed to reproduce Darcy's law.

References

1) Chen, S. and Doolen, G.D.: Annu. Rev. Fluid Mech., **30**(1998), 329
2) Succi, S.: The Lattice Boltzmann Equation for Fluid Dynamics and Beyond, (2001), Oxford University Press
3) Rothman, D.H. and Zaleski, S.: Rev. Mod. Phys., **66**(1994), 1417
4) Buckles, J.J., et al.: Los Alamos Science, **22**(1994), 113
5) Auzerais, F.M., et al.: Geophys. Res. Lett., **23**(1996), 705
6) See for example,
Bear, J.: Dynamics of Fluids in Porous Media, (1988), Dover Publications;
Sahimi, M.: Rev. Mod. Phys., **65**(1993), 1393
7) Frenkel, D. and Smit, B.: Understanding Molecular Simulation, (2002), 465, Academic Press
8) Yamamoto, S. and Hyodo, S.: *Kobunshi-Gakkai Yokoshu* (in Japanese), **51**-3 (2002), 637, Jpn. Soc. Polymer Sci.
9) McNamara, G.R. and Zanetti, G.: Phys. Rev. Lett., **61**(1988), 2332
10) He, X. and Luo, L.-S.: Phys. Rev., **E55**(1997), R6333
11) He, X. and Luo, L.-S.: Phys. Rev., **E56** (1997), 6811
12) Bhatnagar, P.L., et al.: Phys. Rev., **94**(1954), 511
13) He, X., et al.: Phys. Rev., **E57**(1998), R13
14) Martys, N.S., et al.: Phys. Rev., **E58**(1998), 6855
15) Sterling, J.D. and Chen, S.: J. Compt. Phys., **123**(1996), 196
16) Abe, T.: J. Compt. Phys., **131**(1997), 241
17) Shan, X. and He, X.: Phys. Rev. Lett., **80**(1998), 65
18) Wolf-Gladrow, D.A.: Lattice-Gas Cellular Automata and Lattice Boltzmann Models An Introduction, (2000), Springer-Verlag, New York

19) Qian, Y.H., et al.: Europhys. Lett. **17**(1992), 479
20) Mei, R.W. and Shyy, W.: J. Comput. Phys., **143**(1998), 426
21) Buick, J.M. and Created, C.A.: Phys. Rev., **E61**(2000), 5307
22) Guo, Z., et al.: Phys. Rev., **E65**(2002), 046308
23) He, X. and Luo, L.-S.: J. Stat. Phys., **88**(1997), 927
24) See for example, Chapman, S.and Cowling, T.G.: The Mathematical Theory of Non-Uniform Gases, Third Edition, (1970), Chap.7, Cambridge University Press, or, Cercignani, C.: The Boltzmann Equation and Its Applications, (1988), Chap.V., Springer-Verlag, New York
25) Zou, Q. and He, X.: Phys. Fluids, **9**(1997), 1591
26) Ferréol, B. and Rothman, D.H.: Transport in Porous Media, **20**(1995), 3

(Report received on December 26, 2002)

Hidemitsu Hayashi 林秀光
Year of birth : 1954
Division : Digital Engineering Lab.
Research fields : Computational fluid mechanics
Academic degree : Dr. Sci.
Academic society : Phys. Soc. Jpn.